Integrating Artificial Intelligence with Quality by Design in the Formulation of Lecithin/Chitosan Nanoparticles of a Poorly Water-Soluble Drug

Marwa H. S. Dawoud[1] · Islam S. Mannaa[1] · Amira Abdel-Daim[2] · Nabila M. Sweed[1]

Abstract

The aim of the current study is to explore the potential of artificial intelligence (AI) when integrated with Quality by Design (QbD) approach in the formulation of a poorly water-soluble drug, for its potential use in carcinoma. Silymarin is used as a model drug for its potential effectiveness in liver cancer. A detailed QbD approach was applied. The effect of the critical process parameters was studied on each of the particle size, size distribution, and entrapment efficiency. Response surface designs were applied in the screening and optimization of lecithin/chitosan nanoparticles, to obtain an optimized formula. The release rate was tested, where artificial neural network models were used to predict the % release of the drug from the optimized formula at different time intervals. The optimized formula was tested for its cytotoxicity. A design space was established, with an optimized formula having a molar ratio of 18.33:1 lecithin:chitosan and 38.35 mg silymarin. This resulted in nanoparticles with a size of 161 nm, a polydispersity index of 0.2, and an entrapment efficiency of 97%. The optimized formula showed a zeta potential of +38 mV, with well-developed spherical particles. AI successfully showed high prediction ability of the drug's release rate. The optimized formula showed an enhancement in the cytotoxic effect of silymarin with a decreased IC50 compared to standard silymarin. Lecithin/chitosan nanoparticles were successfully formulated, with deep process and product understanding. Several tools were used as AI which could shift pharmaceutical formulations from experience-dependent studies to data-driven methodologies in the future.

Introduction

Pharmaceutical nanocarriers have been extensively investigated as potential drug delivery systems [1] because of their ability to improve the solubility and bioavailability of drugs, which leads to the enhancement of the therapeutic effectiveness of these drugs. Moreover, nanocarriers can control the release of the drug and increase its site specificity to certain organs [2].

The formulation of nanocarriers requires a deep understanding of the product and process, in order to control the variables that may impact the performance of the system. For a successful nanocarrier system, many process and material variables, which may have significant changes during the manufacturing and preparation, should be controlled. Thus, a thorough understanding of the product and the process of its preparation is required in order to produce a robust product and to ensure its continual improvement. Quality by design (QbD) is a strategic product development approach that gives a thorough knowledge about the process and the product understanding. QbD provides complete information about the critical process parameters (CPP) and

linkedin.com/in/marwa-hamdy-1b0656a3

✉ Marwa H. S. Dawoud
  mdawoud@msa.edu.eg; marwa.hamdy@yahoo.com

1 Department of Pharmaceutics, Faculty of Pharmacy, October University for Modern Sciences and Arts, intersection of 26th of July road and Elwahat road, 6th of October city, Giza, Egypt

2 Department of Biochemistry, Faculty of Pharmacy, October University for Modern Sciences and Arts, Giza, Egypt

material attributes (MA) that affect the critical quality attributes (CQA). It results in the creation of design space, which, when controlled, could result in an increase in the robustness and the quality of the product [3]. QbD uses several tools such as risk assessment and Ishikawa diagrams, which lead to the creation of a full quality target product profile (QTPP). One of the powerful tools that could be integrated with QbD is deep learning.

Deep learning is a branch of artificial intelligence (AI) and computer science which focuses on the use of data and algorithms to imitate the way that humans learn [4], which speeds the development process, saves the cost, and keeps the product consistent [5]. It could also help find the non-linear relationships between the independent variables, or between the causal factors and the dependent variables, or between the pharmaceutical responses. Deep learning depends on iterative training of data obtained from a designed experiment [6]. Using deep learning, knowledge and experiences from previous work could be preserved and efficiently used to build models that greatly assist in drug formulations [4].

Cancer accounts for about 10 million deaths worldwide in 2020, as reported by the World Health Organization (WHO) [7]. It remains the major cause of morbidity and mortality, despite decades of basic and clinical research and trials of promising new therapies [8]. Hepatocellular carcinoma (HCC) is the fifth most common cancer worldwide and is estimated to reach 564,000 cases per year. HCC management requires controlling cancer and protecting the liver, to reduce the incidence and mortality rates [7]. However, systemic treatment with anticancer agents could result in many undesirable effects, due to their non-site specificity, which makes them attack normal cells as well [9].

Natural products have gained much attention over the last 40 years in fighting different cancer types. Plant flavonoids, alkaloids, taxoids, and podophyllotoxins are considered from the major resources of these natural compounds, which may have mild side effects on the normal cells [10]. Silymarin, the dry extract of *Silybum marianum*, is a natural flavonoligand and flavonoid that has been widely used in the treatment of different acute and chronic liver toxicities, owing to its hepatoprotective effect. In addition, it has been extensively used in the treatment of inflammation, fibrosis, and oxidative stress. Recently, it was discovered that silymarin has a promising anticancer activity, owing to its anti-proliferation activities through cell cycle regulation, apoptosis induction, chemo-sensitization, growth inhibition, inhibition of angiogenesis, reversal of multi-drug resistance, and inhibition of invasion and metastasis [11]. A major problem with silymarin is its low solubility, which results in its low bioavailability. It has been reported that only 20–50% of orally administered silymarin can be absorbed from the gastrointestinal tract, due to its extensive first pass metabolism and its low solubility [12].

Legalon® and Silipide® capsules are commercially available, which are products containing silymarin. However, these products are rapid-release dosage forms that are administered 3 times daily for a long period of time, which increases the possibility of missed doses [13]. Thus, there is a need to develop a controlled release dosage form that enhances the solubility of silymarin.

Several approaches have been followed to enhance the solubility and, hence, the bioavailability of poorly soluble drugs as dendrimers [14], nanosuspension [15], nanostructured lipid carriers [16, 17], hydrogels [18], and self-emulsifying drug delivery systems [19]. A great attention had been focused on the biodegradable polymers, which overcomes the drug-associated problems [11].

Lecithin chitosan nanoparticles (L/CH) are nanoparticle systems, formed as a result of the supra-molecular self-organizing interaction between the positively charged chitosan and the negatively charged lipids of lecithin. L/CH as drug delivery systems have many advantages due to the use of lecithin, which is a natural lipid mixture of phospholipids and is considered safe and biocompatible and widely used in the fabrication of numerous delivery systems [20], and together with the use of chitosan, being a biocompatible and biodegradable non-toxic cationic polysaccharide which has bioadhesive and penetration-enhancing properties [11]. Several studies were based on loading the drug into L/CH nanoparticles [21–25]. To our knowledge, this is the first study to prepare silymarin-loaded L/CH nanoparticles and to evaluate its efficacy in the treatment of hepatocellular carcinoma

Thus, prediction of % drug release from the L/CH nanoparticles, using deep learning model, is presented in this study.

The objective of the current study is to apply systematic QbD approach integrated with artificial intelligence to fabricate silymarin-loaded L/CH nanoparticles for the treatment of hepatocellular carcinoma and to create a complete QTPP for any L/CH nanoparticle system.

Material and Methods

Material

Silymarin was a generous gift from Sedico Pharmaceutical Company (Cairo, Egypt). Lecithin 90% soybean was purchased from Alfa Aesar (Erlenbachweg 1 Kandel, Germany), while medium molecular weight chitosan and 96% ethanol were obtained from Sigma-Aldrich (St. Louis, MO, USA). Isopropyl myristate was supplied from Loba Chemie (Mumbai, India). All other reagents were of analytical grade and were used as received.

HepG2, a hepatocellular carcinoma cell line, was obtained from Nawah Scientific Inc., (Mokatam, Cairo, Egypt).

Methods

Fabrication of Lecithin/Chitosan Nanoparticles

Self-organized nanoparticles of L/CH were prepared by ionic gelation method as described by Sonvico *et al.*, with slight modifications. Briefly, lecithin and silymarin ethanolic solution were prepared by dissolving accurately weighed amounts of lecithin and silymarin (with or without 0.02% w/v isopropyl myristate (IPM)). This solution was added to 4 mL of 96% ethanol to form 2.5% w/v lecithin/silymarin solution. Chitosan solution 1% w/v was prepared in 1% acetic acid solution and was diluted with distilled water before adding lecithin/silymarin solution, to obtain the required lecithin:chitosan ratio [22]. Lecithin/silymarin ethanolic solution was then injected into 46 mL diluted chitosan solution, using a 0.45-mm inner diameter syringe. Chitosan solution was kept under mechanical stirring at 9000 rpm (Ultraturrax TP 18/10–10N, IKA-Werke GmbH, Staufen, Germany) or water bath sonication (Jiotech UC-10, Serangoon, Singapore), where stirring or sonication was continued for the specified time, with or without heating, to obtain the L/CH liquid dispersion. Blank formulations were prepared as previously discussed but without adding silymarin.

Physicochemical Characterization

Particle size, Polydispersity Index, and Zeta Potential Particle size (PS), measured in terms of hydrodynamic diameters, polydispersity index that measures the particle size distribution (PDI), and zeta potential (ζ-pot) were measured by photon correlation spectroscopy using Zetasizer (Malven Zetasizer version 6.20 serial number: MAL 104 4595, Worcestershire, UK). PS and PDI were measured after suitable dilution in disposable polystyrene cuvettes with scattering angle 25°C. ζ-pot was measured using fixed glass cell, after suitable dilution. A minimum of triplicate samples was used throughout the whole study [25].

Determination of Silymarin-L/CH Interaction Using Infra-red Spectroscopy (IR) Infra-red spectroscopy was used to test the interaction between silymarin and the nanoparticle formulation. Moreover, to ensure the electrostatic interaction between lecithin and chitosan, IR spectrophotometer (Shimadzu, Japan) using KBr pellets, at 25°C with IR source, in the transmission mode, was used to test the absorption bands, in the wave number region from 3500 to 1000 cm^{-1} [26].

Morphological Determination Using Transmission Electron Microscopy Transmission electron microscopy (TEM) (JEM-1400 JEOL, Tokyo, Japan) was used to analyze the morphology of silymarin-loaded lecithin chitosan nanoparticles. One drop of suitably diluted silymarin-loaded L/CH dispersion was deposited on a film-coated copper grid and stained with uranyl acetate and lead citrate. The sample was then allowed to dry for contrast enhancement, and was then morphologically examined using TEM [27].

Determination of Entrapment Efficiency

The entrapment efficiency (EE%) was measured using UV spectrophotometry, after separating the free drug from the entrapped one by centrifugation. One milliliter of the formed dispersion was centrifuged at $14,000 \times g$ at 4°C for 20 min. The supernatant was collected, filtered through 0.22-µm Millipore®, and analyzed spectrophotometrically (using a predetermined calibration curve with a limit of quantification of 2 to 22 µg/mL) after suitable dilution at predetermined $\lambda_{max} = 286$ nm. The entrapment efficiency (EE%) was calculated according to Eq. 1 [28].

$$EE\% = \left(\frac{\textit{Total amount of drug used} - \textit{Amount of drug in supernatant}}{\textit{Total amount of drug used}} \right) \times 100 \tag{1}$$

In Vitro Drug Release Study

In vitro release of silymarin from L/CH nanoparticles was carried out using dialysis bag method at 37°C in a shaking water bath at 100 rpm. *In vitro* drug release was conducted in 100 mL simulated gastric fluid (SGF) at pH 1.2 and in 100 mL simulated intestinal fluid (SIF) at pH 6.8. The optimized formula was compared with the aqueous suspension of silymarin in water (standard). The optimized formula equivalent to 4 mg or standard silymarin was placed in a dialysis bag (molecular weight cut off 12,000–14,000 Da), where the two ends of the bag were firmly clipped and placed in the release medium. A sampling volume of 2 mL was withdrawn at 0, 0.5, 1, 2, 3, 4, 5, 6, 8, 12, 24, and 48 h, and measured spectrophotometrically (using a predetermined calibration curve with a limit of quantification of 2 to 22 µg/mL) at $\lambda_{max} = 286$ nm to determine its concentration. Fresh buffer was added at each sampling interval to attain sink conditions [21]. Each experiment was replicated 3 times.

The *in vitro* release rate of the drug from the formula provides information about the dosage form and its behavior and gives key information about the drug's safety and efficacy [29]. Thus, deep learning is used in this study to predict the % release of the drug at time intervals 2, 8, and 12 h, in order to obtain a data-driven methodology for the % release of any drug from L/CH nanoparticles.

Machine Learning

Pharmaceutical Data The pharmaceutical dataset was extracted from Web of Science, which includes 23 formulations of L/CH nanoparticles. The selected formulation data had similar excipients and processing parameters, except for the drug used. The percentage of the drug released at

time intervals (2, 8, and 12 h) was chosen as the prediction target. The molecular descriptors were used for representing the properties of the active pharmaceutical ingredients. Eight molecular descriptors were used to describe each drug, namely molecular weight, LogP, hydrogen bond donor count, hydrogen bond acceptor count, rotatable bond count, topological polar surface area, heavy atom count, and complexity [5].

Data Splitting Strategy The collected data were split into 3 datasets: they were classified into 60% for training of the model, 20% for validation of the model, and 20% for the testing step, which gave the least errors after training the hyper parameters. The validation dataset was used for tuning the hyperparameters, to get the best model [30]. In order to overcome the drawback of small amount and imbalanced data and to perform the algorithm's performance, a 10-fold cross validation was implemented [31].

Hyperparameters for Deep Neural Network A deep neural network was created using Neural Designer software® V4.2.0. (Artificial Intelligence Techniques, Ltd.). Three models were generated, one for each % release at 2, 8, and 12 h.

Three deep neural networks were generated for each time interval having 3 layers: an input layer with 8 neurons, representing the 8 molecular descriptors; a hidden layer with 2 perceptron layers using a rectified linear unit (ReLu) activation function in 1 perceptron layer; and a linear activation function in the other. In addition, an output layer was represented with a single neuron, corresponding to the % release at the specified time interval, together with a bounding layer, as represented in Fig. 1.

In all networks, a feed-forward neural network with back-propagation was implemented. The optimization algorithm was the Levenberg-Marquardt method, so as to reach a second-order training speed with no need to calculate the Hessian matrix [32]. Overfitting was prevented by early stopping, with a minimum loss decrease and L_2 regularization [33]. A normalized square error was the minimized error function used for all neural networks.

Evaluation Criteria The goodness-of-fit of a statistical model was used for evaluation, which describes how well the data fits a set of observations, showing the relationship between the observed and the expected results through the coefficient of determination, R^2 [34]. Moreover, the expected results were compared with the observed results after performing the *in vitro* release study.

Stability Study

To test the stability of silymarin-loaded L/CH nanoparticles, the PS, PDI, and ζ-pot of the optimized formula were tested after storage of the optimized formula at 4°C and relative humidity of 55–60% for 3 months [35].

Construction of Quality Target Product Profile

Quality target product profile (QTPP) of a drug product could be defined as the whole quality properties needed to be in a drug product to ensure a desired quality product. QTPP ensures achieving safety and efficacy of the drug product, by determination of the proper critical quality attributes (CQA), critical process parameters (CPP), and material attributes (MA) [36]. In case of silymarin formulation, the main target is to enhance the solubility of silymarin, in an attempt to enhance its bioavailability, by formulating silymarin into loaded L/CH nanoparticles. Thus, the highest risk factors affecting the nanoparticle formulation would be a smaller vesicular size, which could increase the drug's solubility, with a smaller PDI to increase the system's homogeneity. In addition, a higher entrapment efficiency might reflect a better performance of the formulation, due to a higher drug loading in the lipidic matrix [36].

Risk Assessment

Risk assessment aims to gather all information about the factors that significantly influence the QTPP. Risk assessment starts with risk identification, which is followed by risk analysis, facilitating the ordering of the potential parameters according to their importance, which contributes to the quality of the final product. This could be hierarchically presented in the form of Ishikawa diagrams.
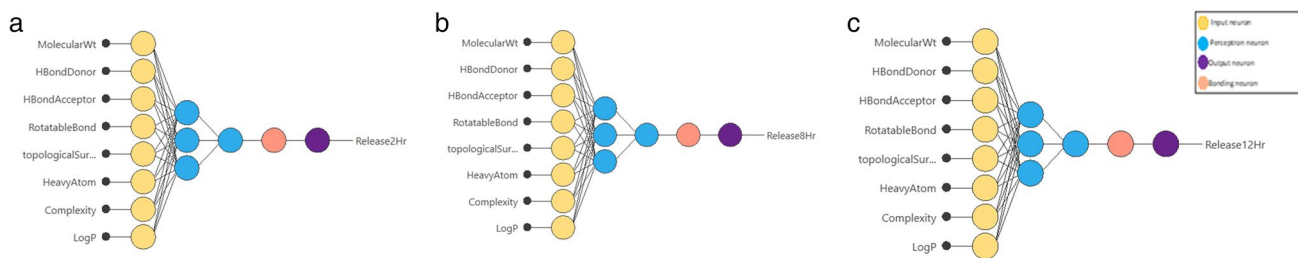

Fig. 1 Final architecture of the neural networks **a** for the release rate at 2 h, **b** for the release rate at 8 h, and **c** for the release rate at 12 h

Table I I-Optimal Design with Results from the Screening Step

CPP/MA			Low level (−1)		High level (+1)				
X_1 L:CH molar ratio			10		40				
X_2 Drug amount (mg)			10		100				
X_3 Mixing time (min)			5		30				
X_4 Heat			Absent		Present				
X_5 Mixing type			Mechanical stirring		Probe sonication				
X_6 Isopropyl myristate			Absent		Present				
Formula c	X_1	X_2	X_3	X_4	X_5	X_6	Y_1: PS (nm)	Y_2: PDI	Y_3: EE (%)
S_1	10	100	30	Present	Stirring	Present	497.5 ± 3.76	0.27 ± 0.09	90.55 ± 2.87
S_2	40	10	30	Present	Sonication	Present	388.7 ± 5.87	0.40 ± 0.07	96.46 ± 5.67
S_3	40	55	5	Present	Stirring	Absent	211.9 ± 8.65	0.37 ± 0.07	84.59 ± 3.76
S_4	10	100	30	Present	Stirring	Present	499.9 ± 4.76	0.21 ± 0.03	90.75 ± 4.17
S_5	10	12.25	5	Present	Sonication	Present	247.5 ± 3.92	0.23 ± 0.08	92.68 ± 8.34
S_6	10	55	30	Absent	Sonication	Absent	446.0 ± 2.31	0.26 ± 0.02	78.46 ± 3.67
S_7	25	10	17.25	Absent	Stirring	Present	196.2 ± 4.76	0.19 ± 0.05	95.99 ± 3.61
S_8	25	10	17.25	Absent	Stirring	Present	201.8 ± 4.87	0.20 ± 0.04	95.11 ± 9.76
S_9	10	55	30	Absent	Sonication	Absent	444.9 ± 5.89	0.29 ± 0.02	78.35 ± 6.90
S_{10}	40	100	30	Absent	Stirring	Absent	340.9 ± 2.87	0.40 ± 0.04	76.64 ± 5.43
S_{11}	40	100	5	Absent	Sonication	Present	154.9 ± 1.98	0.32 ± 0.05	72.69 ± 2.74
S_{12}	40	55	5	Present	Stirring	Absent	215.7 ± 1.73	0.34 ± 0.03	84.22 ± 1.98
S_{13}	40	100	5	Absent	Sonication	Present	166.8 ± 2.93	0.30 ± 0.01	72.28 ± 4.67

Data are expressed as mean ± S.D.

Three main CQA were identified, namely, PS, PDI, and drug EE%, which are assumed to be the most influential factors affecting the nanoparticle formulation [37]. Risk analysis resulted in six CPP/MA, which were studied in the subsequent screening study.

Screening Study Using I-Optimal Design

Based on the results of the risk assessment, 6 CPP/MA were analyzed in screening using I-optimal design. The CPP/MA were X_1, lecithin:chitosan (L:CH) molar ratio [22]; X_2, drug amount [24, 38]; X_3, mixing time [39]; X_4, presence of heat [40]; X_5, mixing type [22, 41]; and X_6, presence of IPM [42], which were all studied at 2 levels. This resulted in the formulation of 13 formulae, as represented in Table I. The levels used were based on previous literature and some preliminary experiments.

Data were analyzed using ANOVA and multi-linear regression, in order to identify the CPP/MA that significantly affected the studied CQA, so as to further proceed to the optimization step.

Optimization Study Using D-Optimal Design

Based on the results from the screening step, two formulation variables—X_1, L:CH molar ratio and X_2, drug amount—were found to be mostly affecting the CQA and, thus, were

deeply studied in the optimization step. Additional 16 formulae were prepared to investigate the potential interaction between the studied MA as tabulated in Table II, where the measured CQA were Y_1, P.S.; Y_2, PDI; and Y_3, EE%.

Data Optimization and Model Validation

Data optimization was successfully achieved depending on desirability criteria, based on a suggested optimized formula (O_1) by the software, with the required constraints to prepare nanoparticles having the smallest PS and PDI, together with the maximum EE%. Accordingly, O_1 was prepared and tested in terms of these constraints, where the observed results were correlated with the suggested results and the % bias was calculated [43].

Design Space and Control Strategy Creation

Design space was created, which shows the relationship between the studied CPP/MA and the CQA. Design space was determined from the common successful operation ranges of the CQA. The successful operating ranges were elucidated from the targeted constraints as stated previously: minimum particle size and PDI with the maximum entrapment efficiency. It is expected to have a product with the desired CQA, when operating within the design space [44]. Furthermore, a control strategy was created, which ensures

Table II D-Optimal Design with Results from the Optimization Step

MA			Low level (−1)	High level (+1)	
X_1 L:CH molar ratio			10	40	
X_2 Drug amount (mg)			10	70	
Formula	X_1	X_2	Y_1: PS (nm)	Y_2: PDI	Y_3: EE (%)
F_1	30.10	15.25	200.5 ± 14.60	0.222 ± 0.02	97.09 ± 3.87
F_2	70	19	309.0 ± 21.60	0.215 ± 0.04	91.39 ± 9.43
F_3	10	25	240.7 ± 5.88	0.215 ± 0.03	92.85 ± 4.67
F_4	10	10	335.0 ± 13.87	0.311 ± 0.07	90.64 ± 1.87
F_5	10	40	343.7 ± 12.12	0.380 ± 0.09	89.18 ± 5.87
F_6	36.10	26.96	131.8 ± 23.65	0.223 ± 0.07	91.84 ± 9.52
F_7	70	40	329.9 ± 3.60	0.265 ± 0.06	87.94 ± 4.76
F_8	70	40	331.9 ± 16.77	0.263 ± 0.08	88.55 ± 3.76
F_9	62.56	29.50	164.9 ± 16.93	0.183 ± 0.07	89.00 ± 5.76
F_{10}	43	40	213.8 ± 15.98	0.260 ± 0.01	83.67± 7.18
F_{11}	51.70	10	281.1 ± 10.82	0.304 ± 0.09	96.32 ± 6.27
F_{12}	70	19	300.7 ± 6.87	0.209 ± 0.04	90.64 ± 7.34
F_{13}	10	40	342.9 ± 11.43	0.371 ± 0.05	88.43 ± 5.87
F_{14}	51.70	10	279.7 ± 14.76	0.306 ± 0.01	96.24 ± 6.98
F_{15}	10	10	283.9 ± 6.87	0.293 ± 0.04	89.83 ± 6.99
F_{16}	50.44	20.20	164.3 ± 23.12	0.132 ± 0.03	93.81 ±3.88

Data are expressed as mean ± S.D.

that the product is consistently and reproducibly produced with required quality [45].

In Vitro Cytotoxicity

Cells were maintained in Dulbecco's modified eagle's medium (DMEM) supplemented with 100 mg/mL of streptomycin, 100 units/mL of penicillin, 10% of heat-inactivated fetal bovine serum in humidified, and 5% (v/v) carbon dioxide atmosphere at 37°C.

Assessment of the Effect of Silymarin as a Free Drug and in the Optimized Formula on the Proliferation of HepG2 Cells The effect of silymarin on the proliferation of HepG2 cells were tested by sulforhodamine B (SRB) assay, which is based on the stoichiometric binding of SRB to the protein. The amount of bound dye indicates the cell mass and can be used as a measure of the cell proliferation [46].

Aliquots of 100 μL cell suspension (5×10^3 cells) were seeded in 96-well plates and incubated in complete media for 24 h. Cells were treated with 100 μL media containing drug (silymarin dissolved in dimethylsulfoxide) at various concentrations, 0.1, 1, 10, 100, and 1000 μM, where the cells were exposed to the drug for 72 h. Fixing of the cells was accomplished by media replacement with 150 μL of 10% trichloroacetic acid (TCA) and its incubation at 4°C for 1 h. This was followed by TCA solution removal and washing of the cells 5 times with distilled water. Aliquots of 70 μL SRB solution (0.4% w/v) were added and incubated in a dark

place at room temperature for 10 min. This was followed by washing of the plates 3 times with 1% acetic acid and air-drying overnight. Then, 150 μL of tris(hydroxymethyl) aminomethane (TRIS) (10 mM) was used to dissolve protein-bound SRB stain, to measure the absorbance at 540 nm using a BMG LABTECH® FLUOstar Omega microplate reader (Ortenberg, Germany). Percentage of cell growth was plotted *versus* the logarithm of drug concentration to determine the half maximal inhibitory concentration (IC_{50}), the drug concentration that causes 50% reduction in the cell growth.

The effects of silymarin as a free drug (standard) and in the optimized formula on the cell cycle of HepG2 cells were analyzed by flow cytometry [47]. HepG2 cells cultured in 12-well plates for 24 h were treated with 100 μL media containing the drug (standard) at a concentration equal to IC_{50} or the optimized formula at the same concentration. After 72 h of drug exposure, cells were detached from plates using the enzyme-free cell dissociation buffer and fixed with 70% ethanol. The nucleic acid content was stained with propidium iodide in RNase-containing buffer and analyzed on FACSVerse. Cell cycle (G0, G1, G2M, and S) was analyzed using FlowJo software (Becton and Dickinson, USA).

Data Analysis

Statistical analysis was performed using Design-Expert 13.0.5.0® software (Stat-Ease Inc., Minneapolis, USA),

which was used in the analysis of I-optimal and D-optimal designs. Responses were analyzed based on linear regression equations and analysis of variance (ANOVA). Several tools were used in the statistical analysis, including comparison of coefficient of variation (CV), multiple correlation coefficient (R^2), adjusted and predicted multiple correlation coefficient (adjusted and predicted R^2), and graphically by 3D response surface plot. A significance was considered at a level of p-value < 0.05 [3]. *In vitro* cytotoxicity and comparisons for deep learning model were analyzed using GraphPad Prism software package, version 9.3.1® (GraphPad Software, Inc., USA). All data was presented as mean ± S.D.

Results and Discussion

Preparation of Lecithin/Chitosan Nanoparticles by Ionic Gelation Technique

A successful formulation of L/CH nanoparticles was achieved by the ionic gelation method. Injection of alcoholic lecithin solution containing silymarin into chitosan solution led to electrostatic interaction between the negatively charged lecithin and the polycationic groups of chitosan. Stable vesicles were formed by self-assembly of the core of lecithin with a shell layer of chitosan, thus protecting the inner structure of the vesicles [21, 48]. It should be noted that the process was spontaneous [49], as evidenced by the turbidity observed when the two solutions were mixed.

FTIR Analysis

The infra-red spectrum of silymarin was analyzed to indicate any interaction with the nanoparticle formulation. As can be observed from Fig. 2c, characteristic peaks of silymarin were observed, where a broad band was observed at 3432 cm^{-1}, corresponding to O-H stretching. Moreover, an absorption band was observed at 1639 cm^{-1} corresponding to C=O stretching [50], which was still present in both the physical mixture (Fig. 2b) and the nanoparticle formulation (Fig. 2a), confirming no interaction between silymarin and L/CH nanoparticles, ensuring its chemical stability.

Furthermore, in order to confirm the interaction between lecithin and chitosan, infra-red spectrum of individual components, their physical mixture, and lyophilized L/CH nanoparticles were analyzed. As can be observed form Fig. 2e, chitosan showed characteristic absorption bands at 1654 cm^{-1}, corresponding to C=O-NHR stretching and another band at 1553 cm^{-1} corresponding to N-H scissoring vibration of primary amino group. Furthermore, a band in the region of 3480–3411 cm^{-1} was observed, which corresponds to N-H and O-H stretching, as well as the intramolecular hydrogen bonds, which were present in the physical mixture (Fig. 2b). The nanoparticle formulation (Fig. 2a) showed the disappearance of these bands indicating the possibility of the electrostatic interaction between the amino group of the chitosan and the phosphate group of the lecithin. Lecithin showed a characteristic peak of P=O at 1230 cm^{-1}, as can be deduced from Fig. 2d, which was present in the physical mixture, and disappeared in the nanoparticle formulation, confirming the interaction.

Quality Target Product Profile

The International Conference on Harmonization (ICH, Q8) covers the steps involved in the pharmaceutical QbD

Fig. 2 FTIR spectrum of(**a** L/CH nanoparticles, **b** physical mixture, **c** silymarin, **d** lecithin, and **e** chitosan
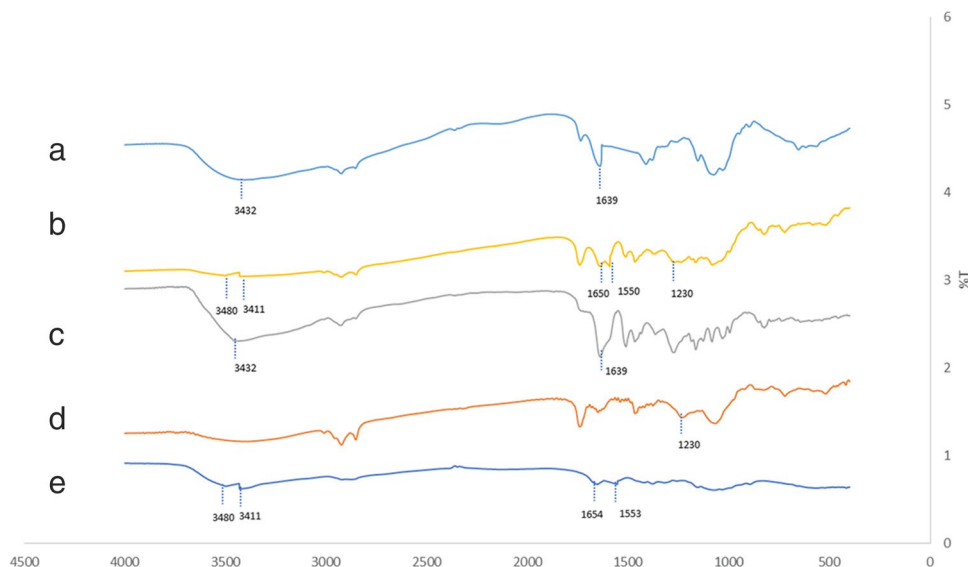
process. It also provides a deep and comprehensive product and process understanding [51]. A diagram of all the steps in the current study involved in the QbD is shown in Fig. 3. The first and most important step in the QbD is to define the QTPP, which describes the quality characteristics of the product, which, when achieved, will accomplish the aim of the study [52]. QbD focuses on establishing a relationship between different variables, which allows a comprehensive understanding of the product and the process. This would finally assure consistent quality with continual improvement [45].

Risk Assessment

The most influential potential factors affecting the CQA were represented and strategically narrowed down by Ishikawa diagrams construction. Accordingly, 2 Ishikawa diagrams were constructed, one showing the most influential factors affecting the PS and PDI and another one for the EE% as demonstrated in Fig. 4. These diagrams were used to gather all the factors affecting each of the CQA. Some of these factors were found to have great impact on the CQA and, thus, were used as the fundamental CPP/MA for the experimental runs, starting from the screening step and ending with the optimization step [53]. The most significant attributes which were used in the screening study were lecithin:chitosan molar ratio, drug amount, time and type of mixing, presence of heat, and using IPM as a solubilizing agent.

As the main target of the current to study is to enhance the solubility of silymarin to be used as an effective anticancer agent, the critical quality attributes considered in this study were the PS of the nanoparticles, and their uniform distribution, in addition to a high entrapment efficiency of the drug.

It is well known that a smaller particle size increases the surface area of the drug exposed to the solvent action and, hence, increases its solubility [54]. Moreover, a small particle size is of great use in targeting the tumor cells, as it has been reported that a vesicular size of less than 400 nm would increase the residence time of the nanoparticles in the systemic circulation and would passively target the tumor cells through enhanced permeability and retention effect [55]. The PDI measures the homogeneity and uniformity of the particle size, and it gives indication about the nanoparticle aggregation and, hence, its stability [56]. Thus, measuring the particle size and the size distribution are considered main attributes. These two CQA can affect the product performance, processability, and stability and, thus, are considered fundamental quality control assays for the product [57]. It is worth noting that a low PDI (<0.4) highly affects the stability and the reproducibility of the release of the drug from the nanoparticles [38].

In similar studies, Lomis *et al.* and Patra *et al.* have reported that higher drug solubility enhances entrapment efficiency, loading capacity, and bioavailability [58, 59]. Thus, the current study aims to minimize each of the PS and PDI and to maximize entrapment efficiency of the drug.

Screening and Analysis of I-Optimal Design

The risk assessment study resulted in 6 CPP/MA that were screened using an I-optimal design, as optimal designs are beneficial in reducing the costs of experimentation. This is because fewer experimental runs are being estimated using statistical models. Moreover, it uses different types of variables, numerical or categorical, with different levels to each factor [60].

Screening is implemented to determine the main effects of the CPP/MA on each of the PS, PDI, and EE%. The

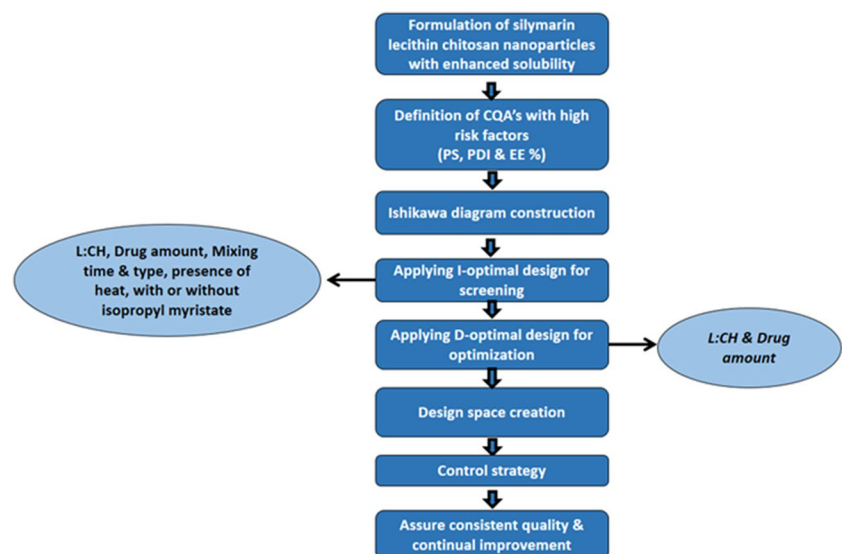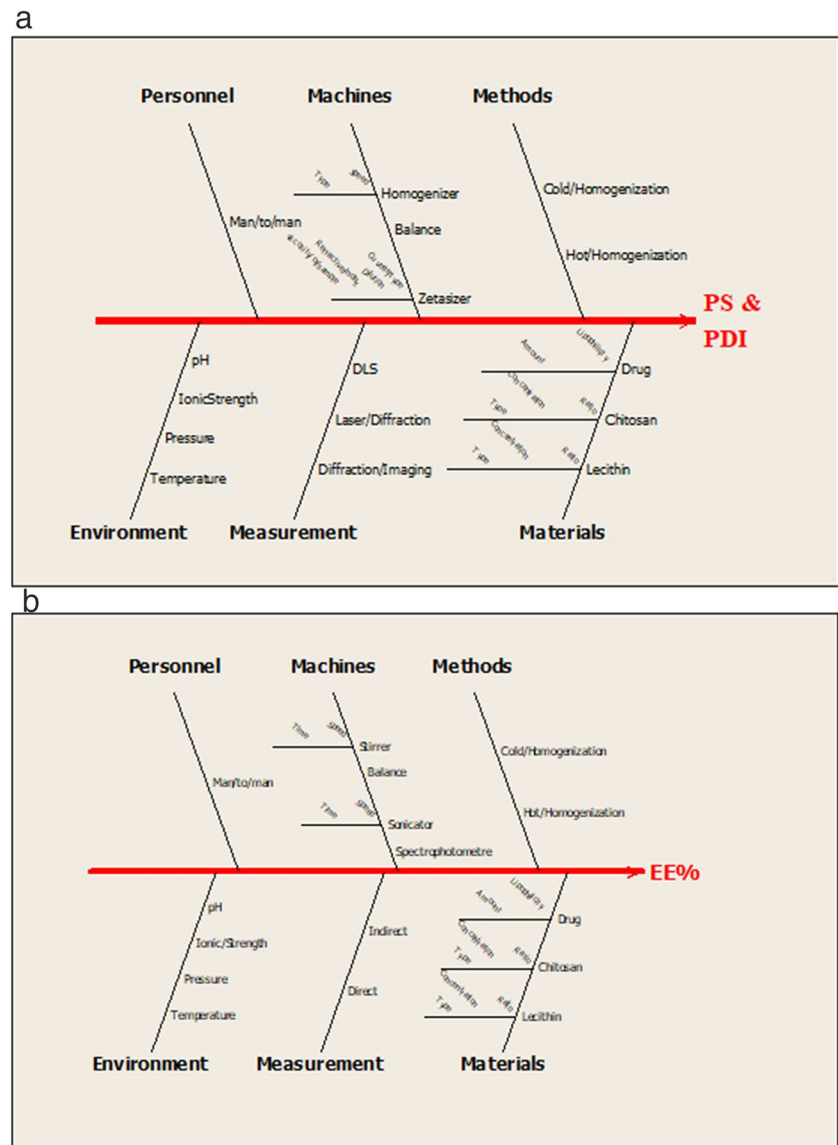**Fig. 3** The steps in QbD for enhancement of the solubility of silymarin

Fig. 4 Ishikawa diagrams for **a** PS and PDI and **b** EE%

software suggested 13 formulae (S_1-S_{13}), which were prepared and measured in terms of the aforementioned CQA as presented in Table I. Table III shows the ANOVA results from the I-optimal design. A significant fitting to the model was observed with a correlation coefficient (R^2) of 0.9964, 0.9385, and 0.9994 for the PS, PDI, and EE%, respectively.

Further analysis revealed that L:CH molar ratio had a significant effect on each of the PS, PDI, and EE%. An increase in the L:CH molar ratio resulted in a smaller particle size, as can be deduced form the negative coefficient of X_1. Furthermore, the increase in the L:CH ratio resulted in a larger PDI and lower entrapment efficiency of the drug. These results were in accordance with several research findings [22, 61–63].

The drug amount significantly affected each of the PS and EE%, where a lower drug amount was more favorable, as it produced a smaller particle size and a higher encapsulation of the drug, as can be observed from Table III.

A shorter time of mixing was preferable for the PS and PDI, as it resulted in a smaller PS and a lower PDI. Thus, the time of mixing will be fixed at the lower level in the subsequent optimization step. Similar results were obtained by Vaezifar *et al.* [39].

The use of heat during the preparation resulted in a bigger PS, a larger PDI value, and a higher entrapment efficiency. This may be due to the fact that thermal treatment might expose more reactive non-polar and sulfhydryl group in the lecithin molecule, which, in turn, increases the hydrophobic attraction and disulfide-bond formation within and between the silymarin and the nanoparticles, which finally increases the vesicular size [64]. Moreover, heating may lead to the evaporation of the residual water that is present in the chitosan solution [40], which may lead to an increase in the chitosan viscosity, which consequently influence the homogeneity of the vesicles [65]. Furthermore, a larger particle

Table III Statistical Analysis of I-Factorial Design

	Y_1: PS (nm)		Y_2: PDI		Y_3: EE %	
	Coefficient	p-value	Coefficient	p-value	Coefficient	p-value
β_0	+309.86	< 0.0001	+0.29	0.0021	+84.88	< 0.0001
X_1 L:CH molar ratio	−39.86	< 0.0001	+0.067	0.0003	−0.67	0.0009
X_2 Drug amount (mg)	+33.02	0.0001	+0.013	0.1965	−6.81	< 0.0001
X_3 Mixing time (min)	+102.51	< 0.0001	+0.030	0.0154	+2.37	< 0.0001
X_4 Heating	+44.52	< 0.0001	+0.028	0.0101	+2.81	< 0.0001
X_5 Type of mixing	+17.97	0.0016	+0.029	0.0151	−3.23	< 0.0001
X_6 Isopropyl myristate	−15.39	0.0034	−0.029	0.0087	+3.49	< 0.0001

size can accommodate more drugs within the nanoparticles, which consequently increases the entrapment of the silymarin [66]. Thus, the formulations in the optimization step will be prepared without heat, as the effect of heat on increasing the PS was more pronounced than its effect on increasing the EE%.

Mechanical stirring showed favorable results over sonication. Using the mechanical stirring resulted in a smaller PS and PDI with higher EE%. The reason for this could be attributed to the effect of sonication that may lead to extensive agglomeration of the nanoparticles, resulting in rapid sedimentation [67], with a larger PS and higher PDI. Moreover, sonication could probably increase the membrane's fluidity of the nanoparticles, which in turn could reduce the entrapment of the drug [68].

Isopropyl myristate was used as a solubilizing agent for the hydrophobic drug silymarin. Thus, the presence of IPM showed very good results as it reduced the PS and PDI and increased the EE%. The lipophilic drug silymarin is mostly present in the lipidic core of the nanoparticles, and the lipid core could be modified by the presence of IPM, which would improve the entrapment of silymarin within the nanoparticles [42]. Moreover, it is well known that the presence of surfactant decreases the particle size due to the reduction in the surface tension, which facilitates the disruption of the droplets [69].

Thus, the screening study resulted in the adjustment of some process variables at certain levels, in order to obtain better results. The best conditions obtained from the I-optimal design were minimal mixing time without heating, using the mechanical stirrer for mixing, and adding IPM. On the other hand, the L:CH molar ratio, together with the drug amount, will be explored in the optimization design in order to evaluate their individual and combined effects.

D-Optimal Design

Statistical Analysis of D-Optimal Design

D-optimal design was the chosen response surface design (RSD) for optimization, as it produces better prediction than I-optimal design [60].

Fitting of the studied model could be indicated by the non-significance of the lack of fit as shown in Table IV. The ANOVA results of all studied CQA for the D-optimal design are shown in Table IV, together with the correlation coefficient (R^2), adjusted and predicted R^2, and the adequate precision. All these values ensure the capability of the model to navigate the design space. As indicated by the high value of correlation coefficient of each CQA (approaching to 1), the close agreement between the studied adjusted and predicted R^2 (less than 0.2 difference), and the high value of the adequate precision (>4) [3], this model could be used to navigate the design space.

Particle Size Analysis

As can be observed from Table II, particle size ranged from 131.8 ± 23.65 to 343.7 ± 12.12 nm. The results indicate an excellent size range for tumor targeting, with enhanced permeability and retention (<400 nm) [55]. Moreover, reduction in the opsonization and detection by the macrophages due to the small vesicular size could result in a longer circulation time [28].

The effect of the MA on the PS, together with the regression equation showing the relationship between the MA and the particle, is presented in Table IV. As can be deduced, the PS was significantly affected by both L:CH molar ratio and the drug amount. A decrease in the L:CH ratio resulted in a larger particle size, as can be deduced from the negative coefficient of X_1 in Eq. 2. However, as the effect was quadratic (Fig. 5a), further analysis showed that there were 2 zones characterizing the effect of L:CH on the PS. At low levels of L:CH, a decrease in the PS was observed. Increasing the L:CH molar ratio may have a direct impact on the vesicular size, which may be attributed to the decrease in the amount of the chitosan [20]. The lower concentration of chitosan would result in a lower viscosity, which might decrease the liquid-phase resistance against dispersion, thus forming smaller nanoparticles [70].

At low levels of L:CH ratio, which means a low amount of lecithin relative to chitosan, enough chitosan would be

Table IV ANOVA Table for the Studied CQA from D-Optimal Design

Source	Y_1: PS					Y_2: PDI					Y_3: EE%				
	Sum of squares	df	Mean square	F value	p-value Prob > F	Sum of squares	df	Mean square	F value	p-value Prob > F	Sum of squares	df	Mean square	F value	p-value Prob > F
Order	Quadratic					Cubic					Cubic				
Model	71,219.39	5	14,243.88	36.19	< 0.0001	0.066	9	7.330E-003	146.11	< 0.0001	188.54	9	20.95	113.62	< 0.0001
$X_1, L{:}CH$	2035.50	1	2035.50	5.17	0.0463	3.617E-003	1	3.617E-003	72.10	0.0001	17.52	1	17.52	95.00	< 0.0001
$X_2, Drug$	2804.20	1	2804.20	7.12	0.0235	4.597E-003	1	4.597E-003	91.63	< 0.0001	2.04	1	2.04	11.08	0.0158
$X_1 X_2$	5333.77	1	5333.77	13.55	0.0042	7.903E-003	1	7.903E-003	157.54	< 0.0001	0.24	1	0.24	1.31	0.2960
X_1^2	28,579.89	1	28,579.89	72.61	< 0.0001	0.031	1	0.031	626.94	< 0.0001	8.03	1	8.03	43.56	0.0006
X_2^2	37,775.68	1	37,775.68	95.97	< 0.0001	2.275E-003	1	2.275E-003	45.35	0.0005	3.13	1	3.13	16.99	0.0062
$X_1^2 X_2$	---	--	---	---	---	9.585E-007	1	9.58E-007	0.019	0.8946	1.88	1	1.88	10.19	0.0188
$X_1 X_2^2$	---	--	---	---	---	4.237E-005	1	4.237E-005	0.84	0.3935	35.35	1	35.35	191.72	< 0.0001
X_1^3	---	--	---	---	---	4.637E-003	1	4.637E-003	92.44	< 0.0001	0.40	1	0.40	2.19	0.1898
X_2^3	---	--	---	---	---	3.789E-003	1	3.789E-003	75.54	0.0001	0.49	1	0.49	2.65	0.1550
Residual	3936.35	10	393.63			3.010E-004	6	5.017E-005			1.11	6	0.18		
Lack of fit	2593.00	5	518.60	1.93	0.2439	7.650E-005	1	7.650E-005	1.70	0.2486	0.035	1	0.035	0.16	0.7033
Pure error	1343.35	5	268.67			2.245E-004	5	4.490E-005			1.07	5	0.21		
Cor total	75,155.74	15				0.066	15				189.65	15			
Regression equation	P.S. = +126.80 − 15.20*X_1 + 17.69*X_2 −29.88* X_{12} + 102.97 * X_1^2 + 119.56* X_2^2 (Equation 2)					PDI = +0.18 + 0.12* X_1 −0.13* X_2 −0.05* X_{12} + 0.12* X_1^2 + 0.03* X_2^2 − 9.72* $X_1^2 X_2$ + 6.54 E-003* $X_1 X_2^2$ − 0.14* X_1^3 + 0.13* (Equation 3)					EE% = + 92.69 −8.32* X_1 − 2.86* X_2 −0.29* X_{12} − 1.93* X_1^2 − 1.21* X_2^2 + 1.36* $X_1^2 X_2$ + 5.98* $X_1 X_2^2$ + 1.33* X_1^3 + 1.52* X_2^3 (Equation 4)				
R^2	0.948					0.995					0.994				
Adjusted R^2	0.921					0.989					0.985				
Predicted R^2	0.880					0.892					0.963				
Adequate precision	18.07					44.01					39.38				

present to cap the growing nanoparticles, preventing its growth, hence a smaller particle size, whereas a further increase in the L:CH ratio, to more than 25:1, will lead to a relative reduction in the availability of the chitosan, which will give a chance for the lecithin nanoparticles to grow, leading to a larger vesicular size [63]. This finding was in accordance with Sonvico *et al.* [22], who attributed the reason for the change in particle size to the aggregation of the particles that could occur at a ratio greater than 30:1. The aggregation was due to the lack of electrostatic stabilization of the L/CH nanoparticles at higher L:CH ratio [22]. Moreover, an increase in the lecithin concentration may lead to stronger electrostatic interaction within the nanoparticles, with subsequent increase in the bilayer of the nanoparticles, which could result in a larger particle size [24].

Furthermore, the PS was significantly affected by the drug amount, where an increase in the PS was observed as the drug amount increased. The particle size showed an initial decrease as the drug amount increased (till 40 µg/mL). By further increasing the drug amount, the PS increased (Fig. 5a). These results were in accordance with Souza *et*
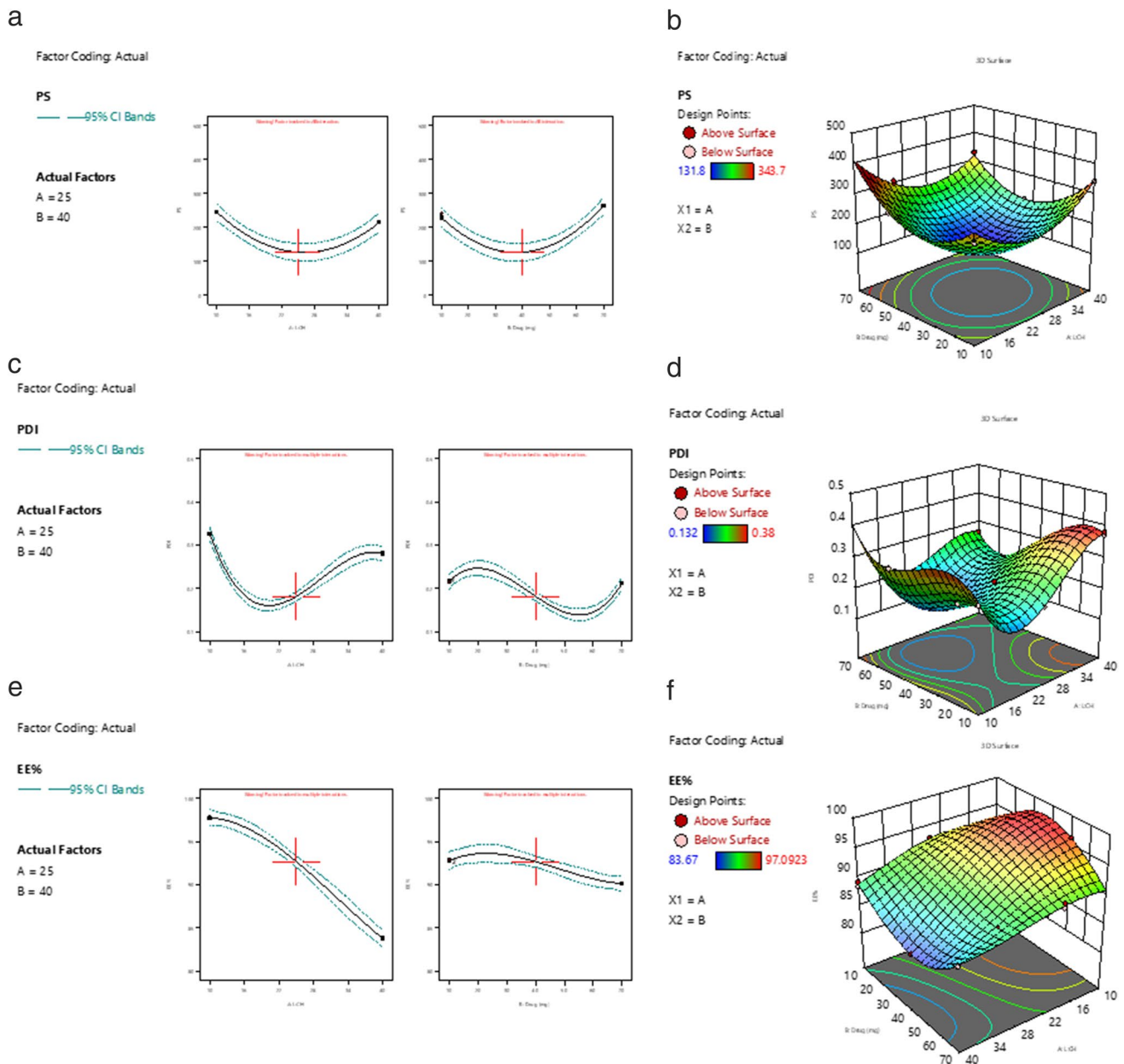
Fig. 5 The effect of the MA on the studied CQA, **a** quadratic effect of each MA on the PS and **b** 3-D plot of the PS, **c** cubic effect of each MA on the PDI and **d** 3-D plot of the PDI, and **e** cubic effect of each MA on the EE% and **f** 3-D plot of the EE%

al. [38], who attributed the increase in the vesicular size at high drug levels to the interference of the drug with the self-assembly of L/CH nanoparticle formation. The repulsive forces may be blocked as a result of the decrease in the spacing between the adjacent nanoparticles. This resulted in more aggregation, which consequently increased the vesicular size [38]. Moreover, the increase in the drug amount above a certain point causes an increase in the viscosity of the disperse phase, with the consequence of forming larger particles [71].

As shown in the 3-D interaction surface plot in Fig. 5b, the PS has a bipolar pattern where PS decreased initially by increasing both the L:CH and the drug amount. This was followed by an increase in PS, when L:CH and drug amount were further increased.

Polydispersity Index Analysis

As mentioned earlier, a uniform monodisperse system is an important attribute for attaining the stability and the targeted delivery of the nanoparticles. As observed in Table II, the PDI range was from 0.132 ± 0.03 to 0.380 ± 0.09, which is considered monodisperse (< 0.4) [38]. As can be observed from Table IV, the PDI was significantly affected by both MA. Further analysis showed a cubic order of interaction. As can be deduced from Fig. 5c, at the low level of L:CH molar ratio (up to 1:20), an initial reduction in the PDI was observed with the increase in L:CH as can be deduced from Eq. 3. It is worth noting that this occurs as far as the chitosan is still sufficient to coat lecithin nanoparticles and will result in a homogenous distribution of the particles, which is achieved at the low L:CH levels. A further increase in the L:CH ratio will reverse the relationship, resulting in a higher PDI. This could be related to the relative increase in the lecithin amount without enough chitosan to coat the nanoparticles, which leads to an increase in the heterogeneity of the system [63].

The amount of silymarin also affected the PDI in a cubic manner as represented in Fig. 5c. At the beginning, nearly no change in the PDI was observed by increasing the drug amount. An increase in the drug amount (>20 mg) resulted in a lower PDI. However, when the drug amount was further increased, the PDI increased. The increase in the PDI with the increase in the drug may be attributed to the increase in aggregation, which could result in the increase in the system heterogeneity [21].

The 3-D plots presented in Fig. 5d show an extreme nonlinear relationship between the PDI and the studied MA, due to their cubic effects, as discussed earlier.

Entrapment Efficiency Analysis

As can be deduced from Table II, the L/CH nanoparticles were capable of entrapping a large amount of silymarin, as the EE% ranged from 83.67 ± 7.18 to $97.09 \pm 3.87\%$. This could be attributed to the high lipophilicity of silymarin, which gives it a big chance to reside in the hydrophobic lecithin nanoparticles. These findings were in agreement with Hafner *et al.*, Şenyiğit *et al.*, and Souza *et al.* [20, 38, 72]. It can be inferred from Eq. 1 that the EE% increases as the L:CH molar ratio decreases. This could be attributed to the higher relative chitosan amount at the low level of L:CH, which is sufficient for capping the lecithin nanovesicles and increasing the tight packing of the particles, thus retaining more drug within and allowing less leakage of the drug [24, 49, 73].

As can be deduced from Fig. 5e, an increase in the drug amount resulted in almost no effect on the EE%, at the beginning. A further drug increase resulted in a lower EE%. This could be because when the drug amount increased, the total amount of polymers present was not enough to solubilize the high level of hydrophobic silymarin, thus resulting in a lower EE% [71, 74].

It should be mentioned that the model showed a cubic order, which is obvious from the 3-D response surface plot, as presented in Fig. 5f.

Optimization, Design Space Creation, and Control Strategy

Construction of a design space was based on preparing L/CH nanoparticles with minimal vesicular size and minimal PDI, together with the maximum EE%. Hence, the design space, shown in Fig. 6, is characterized by two regions: a yellow region, which delivers the desired outcomes if worked within; a grey region, where working within this area will result in undesirable limits. A numerical technique depending on the desirability approach was applied to get an optimized formula with the desirable CQA [52]. Accordingly, a new formula was suggested by the software with a desirability of 0.898. This optimized formula (O_1) was prepared and was tested in terms of the previously mentioned CQA, to create the control space and to check the validity of the design by calculating the % bias. The control space has been created which ensures the reproducibility of the measured and studied attributes.

As can be observed in Table V, the low level of % bias confirmed the validity of the design.

Tests on Optimized Formula for Establishing Control Space

Morphological Structure Using TEM

The micrographs of TEM, as depicted in Fig. 7, show that nanoparticles were in the nanoscale range, with an average size of 115.52 ± 12.71 nm. This was in close agreement with

Fig. 6 Design space for silymarin-loaded L/CH nanoparticles
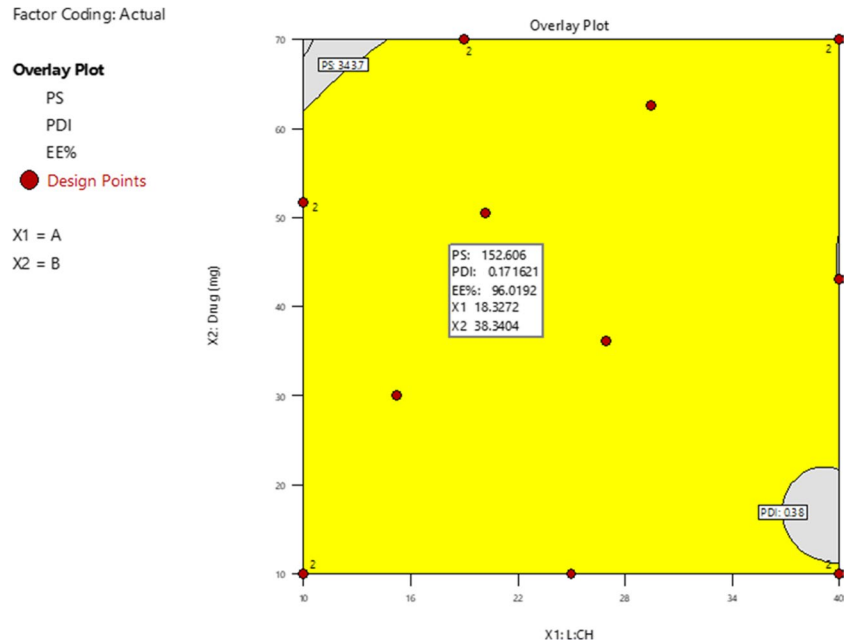
the PS measured by the DLS. The slight difference in the size as determined by DLS method could be due to the difference in the sample preparation [35]. The particles showed a spherical shape, which are almost uniform. The particles were characterized by the presence of a corona surrounding the lecithin nanoparticles, where the drug is most likely to dissolve [42]. It should be noted that the dehydration of the sample might be the reason behind the slightly corrugated surface of the outer shell [67].

Zeta Potential Measurement

The zeta potential was $+38.06 \pm 3.87$ mV. This value indicated the stability of the dispersion, as a zeta potential value above +30 mv indicates the stability of the system, due to the electrostatic repulsion between particles, which prevents their further aggregation [75]. The positive value could be attributed to the cationic chitosan groups on the surface of the vesicles [76]. It is worth noting that the negative value of many nanoparticle systems hinders their use due to their limited cellular uptake [77]. Thus, the formation of positively charged particles is expected to enhance the cellular uptake and, hence, its bioavailability.

In Vitro Release of Silymarin from L/CH Nanoparticles

As the preparation was intended for oral administration, the drug release was tested in both SGF and SIF. As can be observed from Fig. 8, standard silymarin was almost completely released after 3 h in both SGF and SIF. The drug release from the nanoparticles in both media showed a biphasic release, where an initial burst release of the drug followed by a sustained release was observed. This might be attributed to the initial release of the unencapsulated drug, or the drug present on the surface of the vesicles, in addition to the initial swelling of the chitosan that creates pores through which some of the drug is released [78]. This release was followed by a slow passage of the drug out of the nanoparticles core and bilayer [24]. The sustained release pattern could be attributed to the presence of lecithin with a hydrophobic matrix, which may have a great role in improving and prolonging the release of lipophilic drugs [23]. It was observed that the release of silymarin from the nanoparticles in SGF (Fig. 8a) showed a different behavior than that released from SIF (Fig. 8b), where a faster release was observed from the SGF. The reason for this difference might be due to the higher dissolution of chitosan in the acidic

Table V: Optimized Formula with Expected and Observed Results from Response Surface Design

	L:CH molar ratio	Drug amount (mg)	PS	PDI	EE%
	18.331	38.354			
Expected results			152.597	0.172	96.016
Observed results			161.401 ± 6.78	0.204 ± 0.05	97.060 ± 8.76
% Bias*			5.786%	18.604%	1.087%

$*\ \%\ \textbf{bias} = \frac{(|\textbf{Expected}-\textbf{Observed}|)}{\textbf{Expected}} \times \textbf{100}$
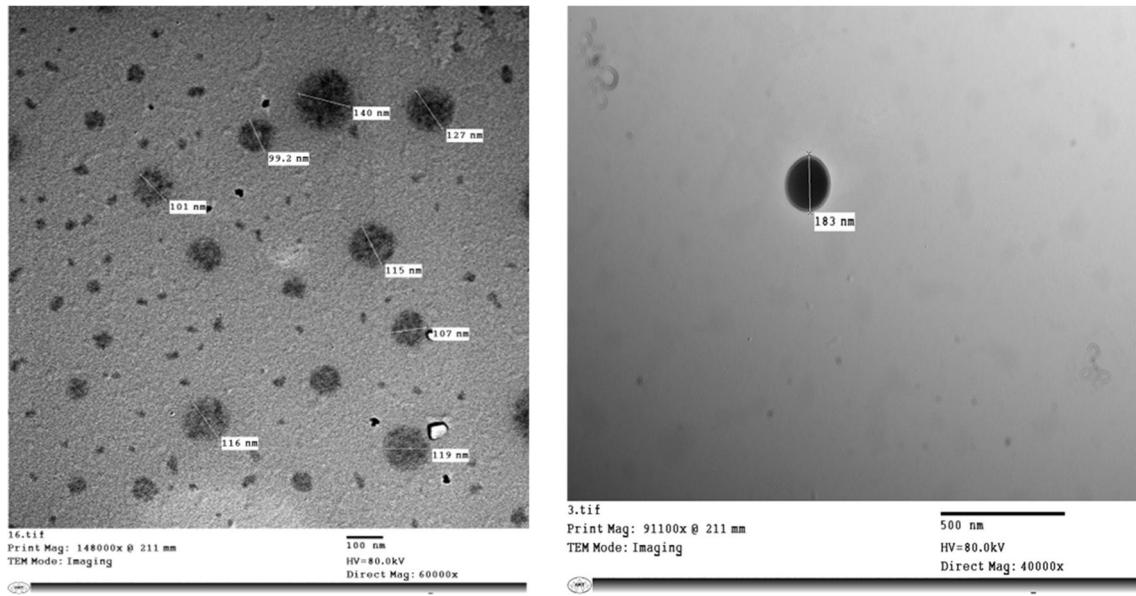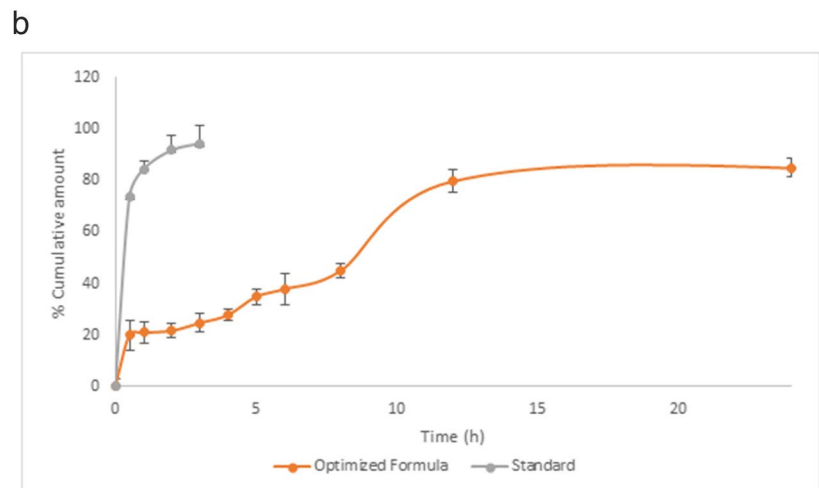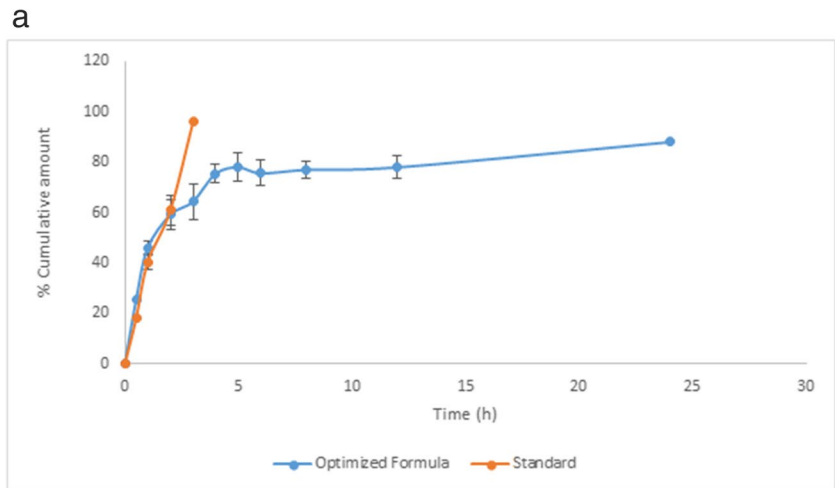
Fig. 7 TEM micrographs of silymarin L/CH nanoparticles

Fig. 8 % Release of silymarin from standard solution and L/CH nanoparticles in **a** simulated gastric conditions and **b** simulated intestinal conditions
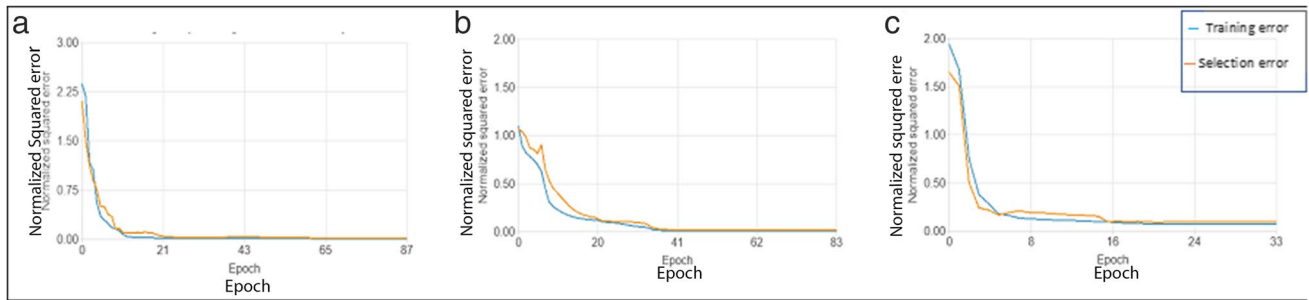
Fig. 9 Levenberg-Marquardt optimization algorithm error history for % release of silymarin from L/CH nanoparticles at **a** 2 h, **b** 8 h, and **c** 12 h

medium [79], which may increase the leakage and, hence, the release of the drug from the nanoparticles [78].

Deep Learning Model for Prediction of the % Release

Deep learning is a type of representation learning with multiple levels of transform modules, which contains more parameters than other learning algorithms [30].

Three models were built for the prediction of the % release of silymarin at 2, 8, and 12 h, respectively, from L/CH nanoparticles, using deep learning models. Optimization of the 3 models was obtained using Levenberg-Marquardt algorithm which was found to be very effective in reducing the errors, as represented in Fig. 9, which shows the training and selection error after each iteration. As shown in Fig. 9a, a training error with an initial value of 2.36812 and a final value of 0.00345765 was observed after 87 epochs for % release at 2 h and an initial value of 2.11435 and a final value of 0.0145122 for the selection error. Moreover, Fig. 9b shows an initial training error of 1.10094 and a final value of 0.00786269 after 83 epochs and an initial selection error of 1.07315 with a final value of 0.0152207 after 83 epochs. Furthermore, Fig. 9c represents an initial training value of 1.93733 ending with 0.072098 after 33 epochs and an initial selection error of 1.65334 and a final value of 0.0930787, for the % release after 12 h.

A goodness-of-fitness test for each time interval showed a very good correlation between the expected and the observed results, as depicted in Fig. 10. A coefficient of determination, R^2, was 0.981, 0.991, and 0.937 for 2 h, 8 h, and 12 h release models, respectively. The values of the expected and the observed results, as shown in Table VI, showed a non-significant difference between the predicted results as obtained from the deep learning model and the experimental results. Thus, the deep learning model for predicting the % release of silymarin from L/CH nanoparticles has been validated and could be used for predicting the % release of any drug form L/CH system at pH 6.8.

Stability Testing

The optimized formula showed insignificant change in PS, PDI, and zeta potential after 3 months, where the PS was 164.56 ± 7.91, the PDI was 0.213 ± 0.09, and the zeta potential was $+37.67 \pm 2.34$ mV, after 3 months of storage at 4°C. Moreover, no evidence of aggregation was observed. This confirms that L/CH nanoparticles have been established at a temperature of 4°C.

In Vitro Cytotoxicity

Silymarin has been used for centuries as a hepatoprotective agent, and its anticancer effect on various malignancies has been reported. Silymarin was proved to suppress the proliferation of a variety of tumor cells, including prostate, ovarian, breast, lung, skin, liver, and bladder [80–84].
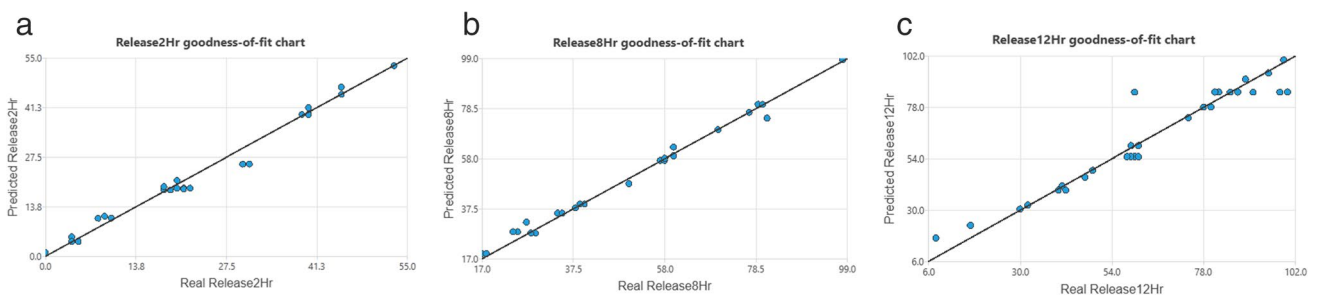

Fig. 10 Goodness-of-fit chart for the deep learning model at **a** 2 h, **b** 8 h, and **c** 12 h

Table VI The Expected and the Observed Results as Obtained from the Deep Learning Model

	Expected	Observed	*p*-value
% Release at 2 h	22.80%	21.78 ± 4.3%	0.8452
% Release at 8 h	43.23%	44.09 ± 3.3%	0.9281
% Release at 12 h	84.98%	79.90 ± 2.4%	0.5397

*Statistically significant

Table VII Effect of Standard Silymarin and Silymarin from the Optimized Formula on Cell Cycle Distribution in Human Hepatocellular Carcinoma Cells (HepG2)

	G1 phase	S phase	G_2/M phase	Sub-Go
Control	50.5 ± 2.0	26.9 ± 2.0	18.8 ± 0.4	1.7 ± 0.6
Standard	59.1 ± 0.8	23.9 ± 0.7	11.8 ± 0.3	3.2 ± 0.1
Optimized formula	55.2 ± 1.1	19.7 ± 0.3*	21.17 ± 1.2	2.8 ± 0.15

Data are presented as mean ± S.D. of percent cell population in different phases of cell cycle

*p-value < 0.05

The effects of silymarin, both as a standard solution and as formulated in L/CH nanoparticles, on the proliferation of HepG2 cells for 72 h were examined by SRP assay. According to Fig. 11 and Table VII, both standard and optimized silymarin significantly (p-value < 0.05) inhibited the growth of HepG2 cells in a concentration-dependent manner, but the optimized formula showed a significant inhibition of the proliferation in the human hepatocellular carcinoma cell line HepG2 more than the standard. A lower IC_{50} of 90.2 μM for silymarin from the optimized formula was observed, while an IC_{50} of 140 μM for standard silymarin was observed. The effects of silymarin on the cell cycle of HepG2 cells as a free drug and in the optimized formula were assessed after exposing the cells to 140 μM for 72 h. A significant suppression of the S phase was observed after treating the HepG2 cell with the optimized formula, but not with the standard. This could be due to the increase in the cytotoxicity of silymarin due to the enhanced cellular uptake when formulated into L/CH nanoparticles. These results were in accordance with [11].

A pervious study by Scambia *et al.* demonstrated the antiproliferative effect of silymarin on gynecological malignancies, including human ovarian and breast cancer cell lines, and showed that silymarin induced G0/G1 phase arrest with a concomitant decrease in the percentage of cells in the S
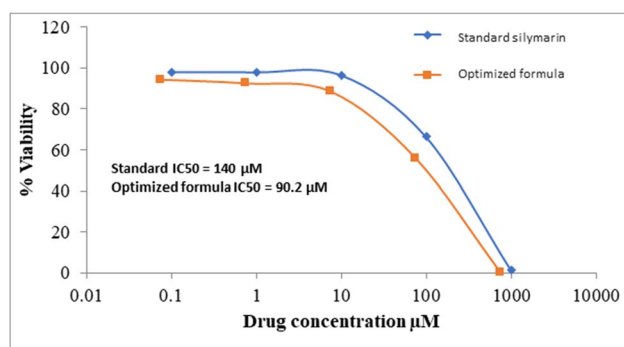
phase of the cell cycle [80]. Sharma *et al.* also showed that silymarin induced growth inhibition and apoptotic cell death in human lung carcinoma cells [85]. Deep *et al.* also reported that silymarin (50–100 μg/mL) inhibited the proliferation of human prostatic carcinoma PC3 cells, induced cell death, and caused G1 cell cycle arrest and suppression of S phase in a dose-/time-dependent manner [86]. Another study done by Ramakrishnan *et al.* also reported the antiproliferative effect of silymarin on the growth of the hepatocellular carcinoma cells, in addition to the increase of apoptotic cell percentage, the proportion of cells with reduced DNA content (Sub-Go peak), and the loss of cells in the G1 phase [87].

Conclusion

Quality by design approach was successfully used in the preparation of silymarin-L/CH nanoparticles, using different tools. A systemized and risk-based approach was adopted for a robust process and product understanding. A risk assessment study was conducted, where Ishikawa diagrams were constructed showing the whole attributes affecting the CQA. Optimal designs were very useful in the screening and the optimization steps, where the screening resulted in the filtration of the CPP/MA from 6 to 2 MA, which were deeply studied in the optimization design. Response surface plots were very useful in interpreting the results, which showed how each of the PS, PDI, and EE% was affected by L:CH and silymarin amount. Artificial intelligence was applied to detect the % release of the drug from the nanoparticle system at various time intervals and showed a great success. A control strategy was established for continual improvement, where the optimized formula was further evaluated for its morphology, zeta potential, drug release, and stability, which all showed promising results. *In vitro* cytotoxicity study showed an enhancement in the cytotoxicity of silymarin when formulated in nanoparticles, with a decreased IC_{50} when compared with standard silymarin. Thus, lecithin chitosan nanoparticles can serve as potential drug carrier for increasing the effectiveness of poorly soluble drugs, where

Fig. 11 Effects of silymarin as standard and in the optimized formula on the proliferation of HepG2 cells. Cells were treated for 72 h with 1000 μM of standard silymarin or from the optimized formula; control cells were treated with DMSO. The cell growth was assessed by SRB assay. The data shown are average of three samples for each treatment

QbD could be applied for the comprehensive understanding of the whole process of preparation. Integrating artificial intelligence into QbD may create a paradigm for pharmaceutical research and industries, transferring studies based on experiences to a new era of methodologies based on data.

Data Availability Raw data were generated at MSA University. Derived data supporting the findings of this study are available from the corresponding author M.H.S. Dawoud on request.

Declarations

Competing Interests The authors declare no competing interests.

References

1. Din FU, Aman W, Ullah I, Qureshi OS, Mustapha O, Shafique S, Zeb A. Effective use of nanocarriers as drug delivery systems for the treatment of selected tumors. Int J Nanomedicine. 2017;5:7291–309.

2. Su S, Kang PM. Recent advances in nanocarrier-assisted therapeutics delivery systems. Pharmaceutics. 2020;12(9):837.

3. Dawoud MHS, Yassin GE, Ghorab DM, Morsi NM. Insulin mucoadhesive liposomal gel for wound healing: a formulation with sustained release and extended stability using quality by design approach. AAPS PharmSciTech. 2019;20(4):158.

4. Xu WJ, Li N, Gao Ck. Preparation of controlled porosity osmotic pump tablets for salvianolic acid and optimization of the formulation using an artificial neural network method. Acta Pharm Sin B. 2011;1(1):64–70.

5. Yang Y, Ye Z, Su Y, Zhao Q, Li X, Ouyang D. Deep learning for in vitro prediction of pharmaceutical formulations. Acta Pharm Sin B. 2019;9(1):177–85.

6. Witek-Krowiak A, Chojnacka K, Podstawczyk D, Dawiec A, Pokomeda K. Application of response surface methodology and artificial neural network methods in modelling and optimization of biosorption process. Bioresour Technol [Internet]. 2014;160:150–160. Available from: https://doi.org/10.1016/j.biortech.2014.01.021.

7. Soerjomataram I, Jemal A, Bray F. Global cancer statistics 2020: GLOBOCAN estimates of incidence and mortality worldwide for 36 cancers in 185 countries. CA Cancer J Clin. 2021;71(3):209–49.

8. Bailar JC, Gornik HL. Cancer undefeated. New England J Med. 1997;336(22):1569–74.

9. Redd WH, Montgomery GH, DuHamel KN. Behavioral intervention for cancer treatment side effects. J Natl Cancer Inst. 2001;93(11):810–23.

10. Demain AL, Vaishnav P. Natural products for cancer chemotherapy. Microb Biotechnol. 2011;4(6):687–99.

11. Pooja D, Babu Bikkina DJ, Kulhari H, Nikhila N, Chinde S, Raghavendra YM, et al. Fabrication, characterization and bioevaluation of silibinin loaded chitosan nanoparticles. Int J Biol Macromol [Internet]. 2014;69:267–273. Available from: https://doi.org/10.1016/j.ijbiomac.2014.05.035.

12. Fenyvesi F, Petervari M, Nagy L, Keki S, Zsuga M, Bacskay L, et al. Solubility increasing experiments of silymarin with cyclodextrins. J Med Aradean. 2011;14(2):13–7.

13. Zeng QP, Liu ZH, Huang AW, Zhang J, Song HT. Preparation and characterization of silymarin synchronized-release microporous osmotic pump tablets. Drug Des Devel Ther. 2016;10:519–31.

14. Huang X, Wu Z, Gao W, Chen Q, Yu B. Polyamidoamine dendrimers as potential drug carriers for enhanced aqueous solubility and oral bioavailability of silybin. Drug Dev Ind Pharm. 2011;37(4):419–27.

15. Cui GJ, Xu LM, Zhou Y, Zhang JJ, Wang JX, Chen JF. Microfluidic fabrication of silybin nanodispersion with high dissolution rate and tunable sizes. Chem Eng J. 2013;222:512–9.

16. Jia L, Zhang D, Li Z, Duan C, Wang Y, Feng F, et al. Nanostructured lipid carriers for parenteral delivery of silybin: biodistribution and pharmacokinetic studies. Colloids Surf B Biointerfaces. 2010;80(2):213–8.

17. Xu P, Yin Q, Shen J, Chen L, Yu H, Zhang Z, et al. Synergistic inhibition of breast cancer metastasis by silibinin-loaded lipid nanoparticles containing TPGS. Int J Pharm. 2013;454(1):21–30.

18. Master AM, Rodriguez ME, Kenney ME, Oleinick NL, Sen GA. Delivery of the photosensitizer Pc 4 in PEG–PCL micelles for in vitro PDT studies. J Pharm Sci. 2010;99(5):2386–98.

19. Wei Y, Ye X, Shang X, Peng X, Bao Q, Liu M, et al. Enhanced oral bioavailability of silybin by a supersaturatable self-emulsifying drug delivery system (S-SEDDS). Colloids Surf A Physicochem Eng Asp. 2012;396:22–8.

20. Hafner A, Lovrić J, Voinovich D, Filipović-Grčić J. Melatonin-loaded lecithin/chitosan nanoparticles: physicochemical characterisation and permeability through Caco-2 cell monolayers. Int J Pharm. 2009;381(2):205–13.

21. Ilk S, Saglam N, Özgen M. Kaempferol loaded lecithin/chitosan nanoparticles: preparation, characterization, and their potential applications as a sustainable antifungal agent. Artif Cells Nanomed Biotechnol. 2017;45(5):907–16.

22. Sonvico F, Cagnani A, Rossi A, Motta S, di Bari MT, Cavatorta F, et al. Formation of self-organized nanoparticles by lecithin/chitosan ionic interaction. Int J Pharm. 2006;324(1):67–73.

23. Alkholief M. Optimization of lecithin-chitosan nanoparticles for simultaneous encapsulation of doxorubicin and piperine. J Drug Deliv Sci Technol. 2019;52(April):204–14.

24. Liu L, Zhou C, Xia X, Liu Y. Self-assembled lecithin/chitosan nanoparticles for oral insulin delivery: preparation and functional evaluation. Int J Nanomed. 2016;11:761–9.

25. Chhonker YS, Prasad YD, Chandasana H, Vishvkarma A, Mitra K, Shukla PK, et al. Amphotericin-B entrapped lecithin/chitosan nanoparticles for prolonged ocular application. Int J Biol Macromol. 2015;72:1451–8.

26. Dawoud MHS, Zaafan MA, Saleh SS, Mannaa IM, Sweed NM. Response surface optimization of a cardioprotective compound through pharmacosomal drug delivery system: in vivo bioavailability and cardioprotective activity potential. Drug Deliv Transl Res. 2023;5:1–25.

27. Tan Q, Liu W, Guo C, Zhai G. Preparation and evaluation of quercetin-loaded lecithin-chitosan nanoparticles for topical delivery. Int J Nanomed. 2011;6:1621–30.

28. Perez-Ruiz AG, Ganem A, Olivares-Corichi IM, García-Sánchez JR. Lecithin-chitosan-TPGS nanoparticles as nanocarriers of (-)-epicatechin enhanced its anticancer activity in breast cancer cells. RSC Adv. 2018;8(61):34773–82.

29. D'Souza S. A review of in vitro drug release test methods for nano-sized dosage forms. Advances in Pharmaceutics. 2014;20(2014):1–12.

30. Yang Y, Ye Z, Su Y, Zhao Q, Li X, Ouyang D. Deep learning for in vitro prediction of pharmaceutical formulations. Acta Pharm Sin B [Internet]. 2019;9(1):177–185. Available from: https://doi.org/10.1016/j.apsb.2018.09.010.

31. Zawbaa HM, Szlęk J, Grosan C, Jachowicz R, Mendyk A. Computational intelligence modeling of the macromolecules release from PLGA microspheres-focus on feature selection. PLoS One. 2016;11(6).

32. Mammadli S. Financial time series prediction using artificial neural network based on Levenberg-Marquardt algorithm. In: Procedia computer science. Elsevier B.V.; 2017. p. 602–7.

33. Simić VM, Rajković KM, Stojičević SS, Veličković DT, Nikolić NČ, Lazić ML, et al. Optimization of microwave-assisted extraction of total polyphenolic compounds from chokeberries by response surface methodology and artificial neural network. Sep Purif Technol. 2016;160:89–97

34. Anderson TW, Darling DA. A test of goodness of fit. A test of goodness of fit. 1954;49(268):765–9.

35. Piazzini V, Landucci E, D'Ambrosio M, Tiozzo Fasiolo L, Cinci L, Colombo G, et al. Chitosan coated human serum albumin nanoparticles: a promising strategy for nose-to-brain drug delivery. Int J Biol Macromol. 2019;129:267–80.

36. Shah B, Khunt D, Bhatt H, Misra M, Padh H. Application of quality by design approach for intranasal delivery of rivastigmine loaded solid lipid nanoparticles: effect on formulation and characterization parameters. Eur J Pharm Sci. 2015;78:54–66.

37. Xu X, Costa AP, Khan MA, Burgess DJ. Application of quality by design to formulation and processing of protein liposomes. Int J Pharm. 2012;434(1–2):349–59.

38. Souza MP, Vaz AFM, Correia MTS, Cerqueira MA, Vicente AA, Carneiro-da-Cunha MG. Quercetin-loaded lecithin/chitosan nanoparticles for functional food applications. Food Bioproc Tech. 2014;7(4):1149–59.

39. Vaezifar S, Razavi S, Golozar MA, Karbasi S, Morshed M, Kamali M. Effects of some parameters on particle size distribution of chitosan nanoparticles prepared by ionic gelation method. J Clust Sci. 2013;24(3):891–903.

40. Szymańska E, Winnicka K. Stability of chitosan - a challenge for pharmaceutical and biomedical applications. Mar Drugs. 2015;13(4):1819–46.

41. Taha A, Ahmed E, Ismaiel A, Ashokkumar M, Xu X, Pan S, et al. Ultrasonic emulsification: an overview on the preparation of different emulsifiers-stabilized emulsions. Trends Food Sci Technol [Internet]. 2020;105:363–377. Available from: https://doi.org/10.1016/j.tifs.2020.09.024.

42. Özcan I, Azizoğlu E, Senyiğit T, Özyazici M, Özer Ö. Enhanced dermal delivery of diflucortolone valerate using lecithin/chitosan nanoparticles: in-vitro and in-vivo evaluations. Int J Nanomed. 2013;8:461–75.

43. Noshi SH, Dawoud MHS, Ibrahim MS. A quality by design approach for the optimization of olmesartan medoxomil-orodispersible lyophilisates: in vitro/in vivo evaluation. J Appl Pharm Sci. 2022;12(06):172–85.

44. Xu X, Khan MA, Burgess DJ. A quality by design (QbD) case study on liposomes containing hydrophilic API: II. Screening of critical variables, and establishment of design space at laboratory scale. Int J Pharm. 2012;423(2):543–53.

45. Basalious EB, El-Sebaie W, El-Gazayerly O. Application of pharmaceutical QbD for enhancement of the solubility and dissolution of a class II BCS drug using polymeric surfactants and crystallization inhibitors: development of controlled-release tablets. AAPS PharmSciTech. 2011;12(3):799–810.

46. Orellana E, Kasinski A. Sulforhodamine B (SRB) assay in cell culture to investigate cell proliferation. Bio Protoc. 22016;6(21):e1984

47. Krishan A. Rapid Flow Cytofluorometric Mammalian Analysis of Iodide Staining. J Cell Biol. 1975;66(1):188–93

48. Dai T, Tanaka M, Huang YY, Hamblin MR. Chitosan preparations for wounds and burns: antimicrobial and wound-healing effects. Expert Rev Anti Infect Ther [Internet]. 2011 9(7):857–879. Available from: http://www.ncbi.nlm.nih.gov/pubmed/21810057.

49. Chuah AM, Kuroiwa T, Ichikawa S, Kobayashi I, Nakajima M. Formation of biocompatible nanoparticles via the self-assembly of chitosan and modified lecithin. J Food Sci. 2009;74(1).

50. Abdullah AS, El Sayed IET, El-Torgoman AMA, Alghamdi NA, Ullah S, Wageh S, et al. Preparation and characterization of silymarin-conjugated gold nanoparticles with enhanced anti-fibrotic therapeutic effects against hepatic fibrosis in rats: role of micrornas as molecular targets. Biomed. 2021;9(12):1767.

51. Guideline IH. Pharmaceutical development. Q8 (2R). As revised in August. 2009;23.

52. Patwardhan K, Asgarzadeh F, Dassinger T, Albers J, Repka MA. A quality by design approach to understand formulation and process variability in pharmaceutical melt extrusion processes. J Pharm Pharmacol. 2015;67(5):673–84.

53. Amasya G, Badilli U, Aksu B, Tarimci N. Quality by design case study 1: design of 5-fluorouracil loaded lipid nanoparticles by the W/O/W double emulsion - solvent evaporation method. Eur J Pharm Sci. 2016;84:92–102.

54. Khadka P, Ro J, Kim H, Kim I, Kim JT, Kim H, et al. Pharmaceutical particle technologies: an approach to improve drug solubility, dissolution and bioavailability. Asian J Pharm Sci. 2014;9(6):304–16.

55. Wilson B, Ambika TV, Dharmesh Kumar Patel R, Jenita JL, Priyadarshini SRB. Nanoparticles based on albumin: preparation, characterization and the use for 5-flurouracil delivery. Int J Biol Macromol. 2012;51(5):874–8.

56. Clayton KN, Salameh JW, Wereley ST, Kinzer-Ursem TL. Physical characterization of nanoparticle size and surface modification using particle scattering diffusometry. Biomicrofluidics. 2016;10(5).

57. Danaei M, Dehghankhold M, Ataei S, Hasanzadeh Davarani F, Javanmard R, Dokhani A, et al. Impact of particle size and polydispersity index on the clinical applications of lipidic nanocarrier systems. Pharmaceutics. 2018;10(2):1–17.

58. Lomis N, Westfall S, Farahdel L, Malhotra M, Shum-Tim D, Prakash S. Human serum albumin nanoparticles for use in cancer drug delivery: process optimization and in vitro characterization. Nanomaterials. 2016;6(6):116.

59. Patra JK, Das G, Fraceto LF, Campos EVR, Rodriguez-Torres MDP, Acosta-Torres LS, et al. Nano based drug delivery systems: recent developments and future prospects 10 Technology 1007 Nanotechnology 03 Chemical Sciences 0306 Physical Chemistry (incl. Structural) 03 Chemical Sciences 0303 Macromolecular and Materials Chemistry 11 Medical and He. J Nanobiotechnology [Internet]. 2018;16(1):1–33. Available from: https://doi.org/10.1186/s12951-018-0392-8.

60. Ranade SS, Thiagarajan P. Available Online through Research Article www. ijptonline. com D VERSUS I OPTIMAL DESIGN: WHAT TO CHOOSE?.

61. Hafner A, Lovrić J, Pepić I, Filipović-Grčić J. Lecithin/chitosan nanoparticles for transdermal delivery of melatonin. J Microencapsul. 2011;28(8):807–15.

62. Liu L, Zhou C, Xia X, Liu Y. Self-assembled lecithin/chitosan nanoparticles for oral insulin delivery: preparation and functional evaluation. Int J Nanomed. 2016;11:761–9.

63. Negi P, Sharma G, Verma C, Garg P, Rathore C, Kulshrestha S, et al. Novel thymoquinone loaded chitosan-lecithin micelles for effective wound healing: development, characterization, and preclinical evaluation. Carbohydr Polym [Internet]. 2020;230(2019):115659. Available from: https://doi.org/10.1016/j.carbpol.2019.115659.

64. Dai L, Sun C, Wang D, Gao Y. The interaction between zein and lecithin in ethanol-Water solution and characterization of zein-Lecithin composite colloidal nanoparticles. PLoS One. 2016;11(11):1–20.

65. Sonvico F, Barbieri S, Rossi A, Motta S, Bettini R, Deriu A, et al. Lecithin-chitosan self-organizing nanoparticles as drug carriers for lipophilic drugs. ImpascienceEu. 2006:4–7.

66. Morsi NM, Aboelwafa AA, Dawoud MHS. Enhancement of the bioavailability of an antihypertensive drug by transdermal protransfersomal system: formulation and in vivo study. J Liposome Res. 2018;28(2):137–48.

67. Dong W, Ye J, Wang W, Yang Y, Wang H, Sun T, et al. Self-assembled lecithin/chitosan nanoparticles based on phospholipid complex: a feasible strategy to improve entrapment efficiency and transdermal delivery of poorly lipophilic drug. Int J Nanomed. 2020;15:5629–43.

68. Nam JH, Kim SY, Seong H. Investigation on physicochemical characteristics of a nanoliposome-based system for dual drug delivery. Nanoscale Res Lett. 2018;13:1–1.

69. Gonzalez RE, Salazar JA, Pérez JA. Obtaining size-controlled microcapsules by ionic gelation with high and low acyl gellans containing Lactococcus lactis. Rev Colomb Biotecnol. 2013;15(2):70.

70. Al-Nemrawi NK, Alsharif SSM, Dave RH. Preparation of chitosan-TPP nanoparticles: the influence of chitosan polymeric properties and formulation variables. Int J Appl Pharm. 2018;10(5):60–5.

71. Sharma N, Madan P, Lin S. Effect of process and formulation variables on the preparation of parenteral paclitaxel-loaded biodegradable polymeric nanoparticles: a co-surfactant study. Asian J Pharm Sci. 2016;11:404–16.

72. Şenyiğit T, Sonvico F, Barbieri S, Özer Ö, Santi P, Colombo P. Lecithin/chitosan nanoparticles of clobetasol-17-propionate capable of accumulation in pig skin. J Controlled Release. 2010;142(3):368–73.

73. Mdlalose WB, Mokhosi SR, Dlamini S, Moyo T, Singh M. Effect of chitosan coating on the structural and magnetic properties of MnFe2O4 and Mn0. 5Co0. 5Fe2O4 nanoparticles. Aip Adv. 2018;8(5).

74. Cooper DL, Harirforoosh S. Effect of formulation variables on preparation of celecoxib loaded polylactide-co-glycolide nanoparticles. PLoS One. 2014;9(12)

75. Ben-David EA, Habibi M, Haddad E, Sammar M, Angel DL, Dror H, et al. Mechanism of nanoplastics capture by jellyfish mucin and its potential as a sustainable water treatment technology. Sci Total Environ. 2023;15:869.

76. Özcan I, Azizoğlu E, Şenyiğit T, Özyazici M, Özer Ö. Comparison of PLGA and lecithin/chitosan nanoparticles for dermal targeting of betamethasone valerate. J Drug Target. 2013;21(6):542–50.

77. Lian D, Chen Y, Xu G, Zeng X, Li Z, Li Z, et al. Delivery of siRNA targeting HIF-1α loaded chitosan modified d-α-tocopheryl polyethylene glycol 1000 succinate-b-poly(ε-caprolactone-ran -glycolide) nanoparticles into nasopharyngeal carcinoma cell to improve the therapeutic efficacy of cisplatin. RSC Adv. 2016;6(44):37740–9.

78. Mohammed MA, Syeda JTM, Wasan KM, Wasan EK. An overview of chitosan nanoparticles and its application in non-parenteral drug delivery. Pharmaceutics. 2017;9(53)

79. Sui X, Zhang H, Yao J, Yang L, Zhang X, Li L, et al. 3D printing of 'green' thermo–sensitive chitosan-hydroxyapatite bone scaffold based on lyophilized platelet-rich fibrin. Biomed Mater (Bristol). 2023;18(2):025022.

80. Scambia G, de Vincenzo R, Ranelletti FO, Panici PB, Ferrandina G, D'Agostino G, et al. Antiproliferative effect of silybin on gynaecological malignancies: synergism with cisplatin and doxorubicin. Eur J Cancer. 1996;32(5):877–82.

81. Korting HC, Megele M, Mehringer L, Vieluf D, Zienicke H, Hamm G, et al. Influence of skin cleansing preparation acidity on skin surface properties. Int J Cosmet Sci [Internet]. 1991 Apr [cited 2017 May 10];13(2):91–102. Available from: https://doi.org/10.1111/j.1467-2494.1991.tb00552.x.

82. Sharma G, Singh RP, Chan DC, Agarwal R. Silibinin induces growth inhibition and apoptotic cell death in human lung carcinoma cells. Anticancer Res [Internet]. 2003;23(3B):2649–55. Available from: http://europepmc.org/abstract/MED/12894553

83. Dhanalakshmi S, Mallikarjuna GU, Singh RP, Agarwal R. Silibinin prevents ultraviolent radiation-caused skin damages in SKH-1 hairless mice via a decrease in thymine dimer positive cells and an up-regulation of p53-p21/Cip1 in epidermis. Carcinogenesis. 2004;25(8):1459–65.

84. Tyagi AK, Agarwal C, Singh RP, Shroyer KR, Glode LM, Agarwal R. Silibinin down-regulates survivin protein and mRNA expression and causes caspases activation and apoptosis in human bladder transitional-cell papilloma RT4 cells. Biochem Biophys Res Commun. 2003;312(4):1178–84.

85. Sharma G, Singh RP, Chan DC, Agarwal R. Silibinin induces growth inhibition and apoptotic cell death in human lung carcinoma cells. Anticancer Res [Internet]. 2003;23(3B):2649–2655. Available from: http://europepmc.org/abstract/MED/12894553.

86. Deep G, Singh RP, Agarwal C, Kroll DJ, Agarwal R. Silymarin and silibinin cause G1 and G2-M cell cycle arrest via distinct circuitries in human prostate cancer PC3 cells: a comparison of flavanone silibinin with flavanolignan mixture silymarin. Oncogene. 2006;25(7):1053–69.

87. Ramakrishnan G, lo Muzio L, Elinos-Báez CM, Jagan S, Augustine TA, Kamaraj S, et al. Silymarin inhibited proliferation and induced apoptosis in hepatic cancer cells. Cell Prolif. 2009;42(2):229–40.